T. A. Thomas, H. C. Nguyen, G. R. MacCartney, Jr., and T. S. Rappaport, "3D mmWave Channel Model Proposal," in *Vehicular Technology Conference (VTC Fall), 2014 IEEE 80th,* Sept 14 - 17, 2014.

3D mmWave Channel Model Proposal

Timothy A. Thomas*, Huan Cong Nguyen†
†Dept. of Electronic Systems, Aalborg University
*Nokia
timothy.thomas@nsn.com, hcn@es.aau.dk

George R. MacCartney Jr., Theodore S. Rappaport
NYU WIRELESS
NYU Polytechnic School of Engineering
Brooklyn, NY 11201
gmac@nyu.edu, tsr@nyu.edu

***Abstract*—There is growing interest in using millimeter wave (mmWave) frequencies for future access communications based on the enormous amount of available spectrum. To characterize the mmWave channel in urban areas, wideband propagation measurements at 73 GHz have recently been made in New York City. Using the measurements, a ray-tracing study has been conducted using databases for the same environments as the measurements, allowing a simple ray-tracer to predict measured statistics such as path loss and angles of arrival in the same physical environment of the measurements. In this paper a preliminary 3GPP-style 3D mmWave channel model is developed with special emphasis on using the ray tracer to determine elevation model parameters. The channel model includes distance-dependent elevation modeling which is critical for the expected 2D arrays which will be employed at mmWave.**

Keywords—channel modeling; 3D channel model; ray tracing; millimeter wave, 73 GHz, channel sounding.

I. INTRODUCTION

Initially, the use of the vast mmWave spectrum concentrated on personal area networks. However, recent experimental and analysis work shows the viability of mmWave for outdoor mobility applications at longer distances up to and exceeding 200 m [1][2][3][4]. Given the enormous amount of spectrum in the mmWave bands, access communications that can provide up to 10,000x capacity over today's systems, and which will be needed by 2030, appears to be realistic [3][4][5]. For example, there is about 10 GHz of available spectrum in the E-band alone, particularly from 71-76 GHz and 81-86 GHz. Hence, there is likely to be a push for standards bodies to create air interface standards for mmWave access communications. In order to adequately assess competing air interfaces, beam alignment procedures, and random access channelization approaches for mmWave communications, a reasonable collection of channel models, for many use case scenarios, must first be developed. The channel models need to have features similar to the 3D channel model developed in 3GPP [6] including distant-dependent elevation angle spreads and elevation angle biases (i.e., elevation angle deviations from the LOS angle), but will require much greater temporal resolution due to the much wider bandwidths than today's LTE standards.

Wideband channel sounders [7][8][9] have been used to measure the reception and departure angles of multipath energy in urban environments, as well as the small scale and large scale multipath spreads and path loss, and early work provides valuable data for creating models in various use cases for mmWave. Additionally, some early channel models have already been proposed for mmWave communications, such as given in [10], which was refined in [11] for use in system-level simulations by including elevation spread. The model in [11] is limited to line of sight (LOS) links confined to an urban street, and is not immediately extendable to the non-line-of-sight (NLOS) links expected for mmWave. Work in [10][11] also did not include several important aspects of the mmWave channel, including polarization and elevation angle biases (i.e., departure from the mean elevation angle).

A second mmWave channel model [4][12] was based on 28 and 73 GHz measurements by NYU [8][9]. In [4][12], a channel model compatible with the existing 3GPP channel model form is proposed, based on numerous measurements in New York City (27 receiver sites for 5 different transmitter (Tx) sites for the 73 GHz measurements for different Tx and receiver (Rx) antennas heights resulted in 74 unique Tx-Rx combinations). The work in [4] [12] is narrowband in nature, and while it deals with large scale path loss models and considers angles of arrival and departure, and angle spread, for a 3GPP-like model, the model does not provide intricate time of arrival or multipath spreads (such work is ongoing at NYU). Given the nascent field of mmWave wireless, there presently is a gap in measurements, including the lack of comprehensive elevation statistics (particularly for Tx departure angles), and there are few measurements accounting for the depolarization of multipath components. Also, the clustering algorithm used in [4][12] likely underestimates the number of clusters since time of arrivals and various Tx elevation angles of departure were not available in the measurement set.

In this paper, we propose a mmWave channel model which attempts to improve on the channel model in [4][12] by using ray-tracing data in the same environment of the NYU measurements, to fill in the gaps in measurement locations, particularly in the elevation dimension. While the ray tracer has not been calibrated to validate the same wideband statistics (e.g., number and statistical distribution of multipath components as measured in the field), the path loss values were tuned for agreement between the ray tracer and the measured data by simple reflection coefficient models. Thus, while preliminary in nature, the resulting channel model, when combined with existing and future measurements, offers the promise to completely characterize the channel in azimuth, elevation, and polarization, and is consistent with the 3GPP ray-based channel modeling methodology and format. The 3GPP modeling is well suited for the generation of static mmWave channels (i.e., without mobile motion which requires channel evolution) since it models all of the expected parameters (e.g., delay, azimuth and elevation angles, polarization) which characterize the expected rays of a mmWave channel.

II. NYU 73 GHz Channel Measurements

Recently, data was collected at 73 GHz in New York City for purposes of characterizing the mmWave urban micro channel [8][9]. The measurements were conducted at 5 transmit sites and 27 receive sites, although we combined the measured data from different Tx heights at each Tx location and considered only a subset of the data at mobile receiver antenna heights. This restricted our analysis to 36 unique Tx-Rx links in the dense-urban environment of downtown New York City, around the NYU campus, where tall buildings, foliage, pedestrians, and vehicular traffic exist. Of interest in this paper were the measurements for access links where the access points (Tx) antennas were 7 m and 17 m above ground and the user equipment (UEs, or Rx locations) antennas were 2 m above ground. More details on the exact locations as well as additional measurements at Rx heights of 4.06 m can be found in [8].

III. Observations from Ray-Tracing

A simple ray tracing environment [14] was designed to identically match the NYU measurements setup. The ray-tracing study area was 600x300 m with a resolution of 2 m between Rx locations. The five Tx locations match the locations of the NYU measurements and four of the Tx locations are at 7 m high and the other is at 17 m. The maximum number of rays is limited to 20 in the ray tracer. An empirical ray tracer is used, which differs from typical ray tracers in that database processing is performed, and empirical interaction losses are modeled in a simple manner, with no accounting for scattered waves. The database processing divides the building walls into tiles for reflections and penetrations, and building edges into vertical and horizontal segments for modeling diffractions (although diffraction is a much weaker propagation mechanism than scattering at 73 GHz). An empirical interaction loss framework is introduced to calculate the reflection, transmission and diffraction losses, instead of using the Fresnel Equation and the uniform diffraction theory. The complete details can be found in [14], but reflection is used as the primary mechanism for propagation.

The basic idea of using a ray tracer is to offer flexibility in simulation while filling in gaps in the channel measurements. For example, due to requirement of directional beamforming at mmWave [2][3][4][9], we need to characterize elevation spread for mmWave. In the field, wideband measurements were made with mechanical rotating horn antennas, and are time consuming, especially for measuring different elevation angles. It was observed in [15] for 2 GHz LTE channels that the elevation spread (i.e., the RMS angle spread relative to the mean elevation angle) is distance dependent and hence it is also likely that it would be distant dependent for mmWave as well. Also, understanding whether other aspects of the elevation parameters, such as cluster elevation spread (i.e., elevation spread of rays which are part of a cluster of rays) and elevation angle bias (i.e., the deviation of the elevation angles from the LOS angle), are also distant dependent and important for proper model creation. Ray-tracing provides an opportunity to easily characterize these effects either without taking additional measurements or until these measurements are available.

After verifying that path loss is properly predicted by the ray tracer as compared with measurements, it is clear that there is strong distance dependence to most of the elevation parameters. For example, the elevation spread of departure (i.e., the RMS spread of the zenith angle of departure (ZoD), where zero degrees zenith represents a Rx antenna pointing directly up in the sky and whereas a zenith of 90 degrees is a Rx antenna pointing on a horizon) versus true propagation distance (3D distance) for all NLOS links simulated in the environment (13,221 different Rx and Tx locations in the ray tracer) is shown in Fig. 1. In Fig. 1, the log[1] of the ZoD spread is shown in the solid blue line and the standard deviation of the log of the ZoD spread is shown in the red dashed line. Overlaid on the data is a line showing the proposed model for both the mean and standard deviation of the log of the ZoD spread (the exact equations are given in Table I). It can be seen that the mmWave ZoD spread is a function of distance, and is adequately modeled using two lines, as was done in the 3GPP 3D modeling [6]. Similar to the 3GPP 3D model, the standard deviation of the log of the ZoD spread can be modeled as a constant. Note that the model for the variance was chosen to match for propagation distances less than 200 m, since the range of interest for mmWave access links may be less than this amount, and measurements in [8] were limited to within 200 m.

The mmWave ZoA (zenith angle of arrival) spread is also distance dependent and can be modeled similarly to the ZoD spread. The cluster ZoA and ZoD spreads were found to have a distance dependence, as well. The ray clustering algorithm described in [16] was used here, and the clusters are determined considering the time of arrivals, the azimuth and elevation angles of arrival and departure, and the ray powers of the ray tracing simulations. Thus the finest granularity of clustering is obtained here, which is important when using a 3GPP-style channel model. Further refinement through comparison of the measured multipath arrivals and strengths with the ray traced data is needed to validate the clustering results here, (this shall be the subject of subsequent work), but the present formulation is a useful step for a mmWave 3GPP-like model for elevation effects.

In addition to the above parameters, the mmWave ZoA and ZoD biases also exhibit distance dependence, as seen in Fig. 2. It turns out that there tends to be a positive angle bias, meaning that the NLOS channel rays tend to depart and arrive higher in elevation than the LOS ray. This observation was also made for the NYU 28 GHz propagation data, where in many NLOS locations, it was best for the RX to look up at 20 degrees as opposed to on the horizon or at 20 degrees below the horizon (towards the ground) [7]. Hence, it is best to model the log of the negative bias as being piece-wise linear, with the standard deviation of the log of the negative bias being constant, as for the elevation spreads. The full details of the distance dependence of these parameters are given in the next section and Table I.

One gap in both the ray-tracing simulations and the NYU measurements is the ability to model polarization. While a few

[1] Unless otherwise noted, log will refer to the base-ten log and ln will be used for log base *e*.

cross-polarized LOS measurements in [8] showed 25-30 dB cross-polarized discrimination (XPD), here we use the XPD results from [17] and assume a statistical XPD with a mean of 15 dB with a standard deviation of 2 dB. In addition, a modification to the polarization dyadic (the dyadic is the 2x2 matrix as in the subsequent equation (1) which characterizes the polarization between vertical (or theta) and horizontal (or phi) polarizations in the channel) relative to the 3GPP modeling [6] is done for our proposed mmWave model to better accommodate circular polarization. The findings of [18] and earlier microwave work [19] shows that a single reflection changes from right-hand circular polarization to left-hand circular polarization, whereas two successive reflections retain the original polarization. Future measurements will enable us to refine polarization modeling.

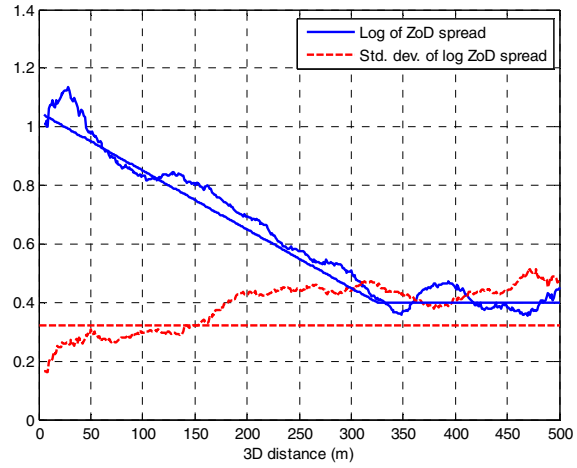

Fig. 1. Log of the ZoD spread (solid line) and standard deviation of the log of the ZoD spread as a function of 3D distance for NLOS links. The proposed piecewise linear model is overlaid on the ray-tracing results.

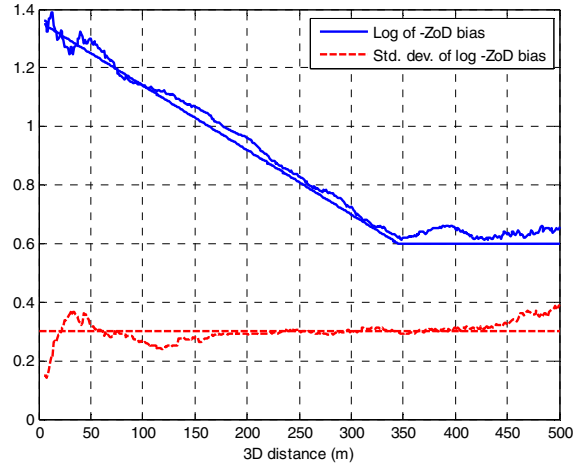

Fig. 2. Log of –ZoD bias (solid line) and standard deviation of the log of -ZoD bias as a function of 3D distance for NLOS links. The proposed model is overlaid on the ray-tracing results.

IV. Proposed Channel Model

We now present a channel model for the urban micro (UMi) environment based on the ray-tracing data. In addition, where the ray tracer has deficiencies (particularly in the number of rays available for determining azimuth angle spreads), the parameters the model uses are modified to better match the measured data. It turns out that for most parameters a fine tuning based on the measured data was not necessary since the channel model derived from the ray tracer matched the statistics of the measured data well. The one exception was for the azimuth angle of arrival (AoA) statistics where the ray tracer failed to account for the scattering in the channel, and thus showed lower AoA spread than the measured data from [7][8]. Thus, our channel model uses a higher AoA spread than predicted by the ray tracer. Also the elevation parameters were all derived from the ray tracer since the channel measurements did not have sufficient measurements in elevation. The details of all of the model parameters are given in Table I, and Table II shows the cross-correlations of the large-scale parameters (e.g., delay spread to AoA spread, AoA spread to AoD spread, etc.) as derived from the ray-tracing data. The cross correlations deviate from the UHF 3GPP cross-correlations in that the correlation of shadow fading to the other large-scale parameters and the Ricean K factor to the other large-scale parameters is not considered to simplify the model. In their place the cross-correlation of the elevation angle biases to the other large scale parameters is considered. This is a departure from the UHF 3GPP modeling where no cross-correlation to the elevation angle biases was considered.

The goal of the NLOS channel model is to generate all of the parameters needed to obtain a wideband impulse response channel for each cluster as:

$$\mathbf{H}_{u,s,n}(t) = \sqrt{P_n}\sum_{m=1}^{M}\begin{bmatrix} F_{rx,u,V}(\varphi_{n,m},\zeta_{n,m}) \\ F_{rx,u,H}(\varphi_{n,m},\zeta_{n,m}) \end{bmatrix}^T \times \begin{bmatrix} e^{j\Phi_{n,m}^{vv}} & \sqrt{\kappa_{n,m}^{-1}}\,e^{j\Phi_{n,m}^{vh}} \\ \sqrt{\kappa_{n,m}^{-1}}\,e^{j\Phi_{n,m}^{hv}} & e^{j\Phi_{n,m}^{hh}} \end{bmatrix} \begin{bmatrix} F_{tx,s,V}(\phi_{n,m},\theta_{n,m}) \\ F_{tx,s,H}(\phi_{n,m},\theta_{n,m}) \end{bmatrix}, \quad (1)$$
$$\times e^{j2\pi\lambda_o^{-1}(\bar{\varphi}_{n,m}\cdot\bar{r}_{rx,u})}\, e^{j2\pi\lambda_o^{-1}(\bar{\phi}_{n,m}\cdot\bar{r}_{tx,s})}\, e^{j2\pi\upsilon_{n,m}t}$$

where u is the u^{th} mobile receive antenna, s is the s^{th} base transmit antenna, n is the cluster number, P_n is the power of cluster n, M is the number of rays per cluster, $F_{rx,u,v}$ and $F_{rx,u,H}$ are the field antenna patterns for the u^{th} mobile antenna in 3D for the vertical and horizontal (aka theta and phi) polarizations respectively, $\varphi_{n,m}$ is the azimuth angle of arrival, $\zeta_{n,m}$ is the elevation angle of arrival, κ is the cross polarization power ratio in a linear scale, $\Phi_{n,m}^{vv}$, $\Phi_{n,m}^{hv}$, $\Phi_{n,m}^{vh}$, $\Phi_{n,m}^{hh}$ are the phase values for all four polarization combinations, $F_{tx,s,v}$ and $F_{tx,s,H}$ are the field antenna patterns for the s^{th} base antenna in 3D for the vertical and horizontal (aka theta and phi) polarizations respectively, $\phi_{n,m}$ is the azimuth angle of departure, $\theta_{n,m}$ is the elevation angle of departure, λ_o is the wavelength, $\bar{\varphi}_{n,m}$ is a unit vector pointing in the direction of azimuth and elevation angles of arrival, $\bar{r}_{rx,u}$ is a vector of the positions of the u^{th} mobile antenna, $\bar{\phi}_{n,m}$ is a unit vector pointing in the direction of the azimuth and elevation angles of departure, $\bar{r}_{tx,s}$ is a vector of the positions of the s^{th} base antenna, and $\upsilon_{n,m}$ is the Doppler frequency given as in equation (24) in [6] and is copied here for completeness:

$$\upsilon_{n,m} = \frac{\overline{\varphi}_{n,m}^T \overline{v}}{\lambda_o} \quad , \quad \overline{v} = v_s[\sin\theta_v \cos\phi_v \;\; \sin\theta_v \sin\phi_v \;\; \cos\theta_v]^T$$

where v_s is the speed (m/s), ϕ_v is azimuth travel angle, and θ_v is the elevation travel angle.

The detailed steps to create the mmWave channel are similar to [6] and are summarized now[2]:

1. Set up the simulation environment (e.g., UE and access point locations, antenna array configurations, sectorization strategy, building/foliage locations).
2. Choose a propagation condition, LOS or NLOS, based on blockage between the UE and access point.
3. Calculate the omni-directional path loss as:
$$PL[dB](d) = 20\log_{10}\left(\frac{4\pi}{\lambda_o}\right) + 10n_{pl}\log_{10}(d) + \sigma_{SF}$$
where λ_o is the wavelength, n_{pl} is the path loss exponent, d is the distance in m, and σ_{SF} is the shadow fading (as given in Table I). For 73 GHz it was found that n=2.1 and σ_{SF}=4.9 dB for LOS and n_{pl}=3.3 and σ_{SF}=7.6 for NLOS [5]. Note that this path loss formula is a reference-distance-based formulation where the reference distance is 1 m.
4. Generate the large scale parameters (σ_τ, etc.) as correlated Gaussian random variables using Table I to generate the parameters and Table II to cross-correlate them. In other words, generate seven zero-mean unit-variance Gaussian random variables, $x(1)$ through $x(7)$, that are correlated using the parameters in Table II. Then, for example assuming $x(1)$ is associated with the delay spread, $\sigma_\tau = 10^{\varepsilon_{DS}x(1)+\mu_{DS}}$. Limit the AoD and AoA spreads to 100 degrees, the ZoD and ZoA spreads to 40 degrees, and the elevation bias to -75 degrees.
5. Generate the cluster delays with an exponential distributions: $\tau_n = -r_\tau \sigma_\tau \ln(X_n)$ where r_τ is the delay scaling parameter from Table I, and X_n is an unit-variance Gaussian random variable. Sort the delays: $\tau_n = \text{sort}(\tau_n - \min(\tau_n))$. Next, generate the per-cluster delays as:
$$\tau_{n,m} = \begin{cases} \tau_n, & m = 1,2,3,4 \\ \tau_n + 5\ n\text{sec}, & m = 5,6,7 \\ \tau_n + 10\ n\text{sec}, & m = 8,9,10 \end{cases}$$
6. Generate the cluster powers as:
$$P_n = \exp\left(-\tau_n \frac{r_\tau - 1}{r_\tau \sigma_\tau}\right) \cdot 10^{-0.1Z_n}$$
where Z_n is $N(0,\zeta^2)$ and ζ is the per-cluster shadow fading from Table I. Normalize the powers so the sum is one.
7. Generate the AoAs and AoDs as (the same procedure is used for both so only the AoD procedure is given):
$$\phi'_{n,AoD} = 2.33(\sigma_{ASD}/1.4)\sqrt{-\ln(P_n/\max(P_n))}$$
$$\phi_{n,AoD} = X_n \phi'_{n,AoD} + Y_n + \phi_{LOS,AoD}$$
where $\phi_{LOS,AoD}$ is the LOS AoD angle, Y_n is $N(0, \sigma_{ASD}^2/49)$, and X_n is either +1 or -1 with equal probability. Create the angles within a cluster as:
$\phi_{n,m,AoD} = \phi_{n,AoD} + c_{ASD}\alpha_m$ with α_m taken from Table III and c_{ASD} being the cluster ASD spread from Table I.
8. Generate the ZoAs and ZoDs as (the same procedure is used for both so only the ZoD procedure is given):
$$\theta'_{n,ZoD} = -1.01\sigma_{ZSD}\ln(P_n/\max(P_n))$$
$$\theta_{n,ZoD} = X_n \theta'_{n,ZoD} + Y_n + \theta_{LOS,ZoD} + \mu_{bias,ZoD}$$
where $\theta_{LOS,ZoD}$ is the LOS ZoD angle, Y_n is $N(0, \sigma_{ZSD}^2/49)$, X_n is either +1 or -1 with equal probability, and $\mu_{bias,ZoD}$ is generated as:
$\mu_{bias,ZoD} = \max(-10^{\mu_{ZBD}+X\varepsilon_{ZBD}}, -75)$ where X is N(0,1) cross-correlated with the other parameters as described in Step 4 and μ_{ZBD} and ε_{ZBD} are given in Table I.
Create the angles within a cluster as:
$\theta_{n,m,ZSD} = \theta_{n,AoD} + c_{ZSD}\alpha_m$ with α_m taken from Table III and c_{ZSD} being the cluster ZSD spread from Table I.
9. Within a cluster randomly couple all of the AoD, AoA, ZoA, and ZoD angles by randomizing the order of each group of angles within a cluster (e.g., using Matlab's randperm(10) within each group of angles within a cluster).
10. Generate the XPRs as $\kappa_{n,m} = 10^{X/10}$ where X is Gaussian distributed with the parameters in Table I.
11. Generate the random phases for the dyadic term, $\Phi_{n,m}^{vv}$, $\Phi_{n,m}^{vh}$, $\Phi_{n,m}^{hv}$, $\Phi_{n,m}^{hh}$. To accommodate the behavior of polarization and especially the circular polarization mentioned in the last section, set $\Phi_{n,m}^{hh} = \Phi_{n,m}^{vv} + X_n\pi$ where X_n={0,1} and is meant to characterize the interactions with a number of reflections for the given cluster.

When generating a LOS channel, a NLOS channel is first generated using the procedures in steps 4-11 given above, and then a LOS ray is added to that channel based on the Ricean K factor draw (given by the parameters in Table I). Note that for simplicity the Ricean factor is assumed to be uncorrelated with the other parameters. The Ricean factor is used to scale the LOS ray relative to the generated NLOS channel and the sum of the average power in the LOS portion plus the average power in the NLOS should be one. The angles for the LOS ray are for the direct path between the Tx and Rx and the delay of the LOS ray is 0. For the LOS ray, the XPR value is set to infinity (i.e., the off-diagonal terms of the dyadic are zero) and $\Phi_{n,m}^{vv} = \Phi_{n,m}^{hh} + \pi$.

V. Channel Model Comparisons to NYU Data

In this section we compare statistics of the proposed channel to the NYU measured data for UEs at 2 m high. For the simulated channel, the conditions were chosen similar to the

[2] Note that by purposeful design, these procedures read similarly to [6].

NYU measurements with a minimum distance of 50 m and a maximum distance of 200 m. When viewing these results we kept in mind that for low 2 m Rx heights, the NYU measurements consisted of 10 unique Tx-Rx locations for LOS and 31 unique Tx-Rx locations for NLOS, meaning there was a relatively limited amount of data to compute the statistics.

Fig. 3 shows a comparison of the RMS delay spread for the best beams at both the Tx and Rx. In both the simulated channels and the NYU data, the Tx and Rx side had 7 degree beamwidth antennas in the azimuth and elevation planes. The antennas were scanned at various angle conventions and the Tx-Rx angle combinations that had the highest receive power were used to collect the delay statistics. In both the LOS and NLOS locations, the model produced similar results to the measured data, thus no fine tuning of the time of arrivals was needed.

Fig. 4 shows a comparison of the RMS AoD spread for the NYU data and the channel model when considering omni-directional antennas at both ends. Good match is obtained except maybe for some LOS measurements, but given the small data set, there is not enough evidence that fine-tuning of the AoD spreads is needed. On the other hand, fine tuning was needed for AoA spreads, since the AoA spreads from the ray tracer were 25 to 50% lower than what the NYU measurements showed. Fig. 5 shows a comparison of the AoA spreads after the fine tuning of the model. The NLOS has reasonable alignment with the NYU measurements, but the LOS NYU measurements are higher than the NLOS, which may be due to scattering and stronger sidelobe reflections in the LOS urban canyon.

The elevation spreads for the NYU measured channels were all much lower than the channel model produces, but this is expected as the current channel measurements will underestimate the elevation spreads. Hence for the elevation parameters, the ray-tracing results were used without any fine tuning from the NYU measurements.

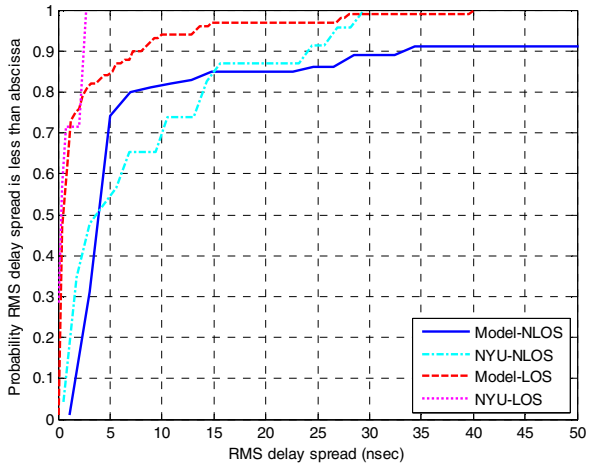

Fig. 3. Comparison of RMS delay spreads for the best beams at the Tx and Rx for channel model versus the NYU data measurements.

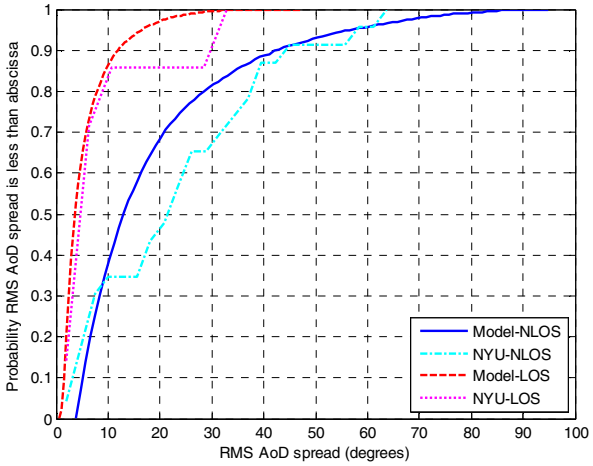

Fig. 4. Comparison of AoD spreads for channel model versus the NYU data measurements.

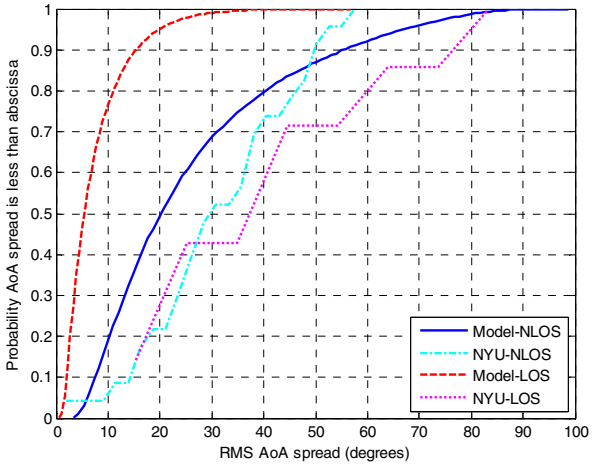

Fig. 5. Comparison of AoA spreads for channel model versus the NYU data measurements.

VI. Future Work

Some further tuning of the model may be necessary given the gaps in measured data, and also limitations of the ray tracer used. First, implementation of the scattering phenomenon, and a better understanding of the depolarization of rays in the NLOS environment is needed. Second, more elevation measurements are needed to ensure that the elevation dimension is modeled properly. Third, a study on the correlation distances at mmWave needs to be made. Finally, an investigation into the cross-correlation of shadow fading and/or Ricean factor with the other parameters may be desired.

VII. Conclustion

In this paper we proposed a ray-based channel model for mmWave communications in an urban-micro setting. The channel model was derived from ray-tracing data where the path loss values were tuned for agreement between the ray tracer and measurements taken at 73 GHz in New York City. The channel model follows a similar structure to the recently-finalized 3GPP 3D channel model enabling simple implementation for simulators capable of generating the 3GPP 3D channels. The statistics of the proposed model were shown to be consistent with the statistics of the measured channels, al-

though scattering and refined ray tracing improvements, along with better tuning with measurements, will offer further improvements.

REFERENCES

[1] T. S. Rappaport, J. N. Murdock, F. Gutierrez, "State of the art in 60-GHz integrated circuits and systems for wireless communications," *Proc. of the IEEE*, Vol. 99, No. 8, August 2011.

[2] T. S. Rappaport, et. al., "Broadband millimeter-wave propagation measurements and models using adaptive-beam antennas for outdoor urban cellular communications," *IEEE Trans. on Antennas and Propagation*, Vol. 61, No. 4, April 2013.

[3] T. S. Rappaport, et. al., "Millimeter Wave Mobile Communications for 5G Cellular: It Will Work!", *IEEE Access*, Vol. 1, May 2013.

[4] S. Rangan, T. S. Rappaport, E. Erkip, "Millimeter-wave cellular wireless networks: potentials and challenges," *Proc. of the IEEE*, Vol. 102, No. 3, March 2014.

[5] A. Ghosh, et. al., "Millimeter Wave Enhanced Local Area Systems: A high data rate approach for future wireless networks," *IEEE Journal on Sel. Areas in Comm*., Special Issue on 5G, July, 2014.

[6] 3GPP TR 36.873, v1.3.0, "Study on 3D channel model for LTE (Release 12)", February, 2014 (available at www.3gpp.org).

[7] M. Samimi, et. al., "28 GHz angle of arrival and angle of departure analysis for outdoor cellular communications using steerable-beam antennas in New York City," *in Proc.IEEE VTC-Spring*, 2013.

[8] G. R. MacCartney and T. S. Rappaport, "73 GHz Millimeter Wave Propagation Measurements for Outdoor Urban Mobile and Backhaul Communications in New York City," *in Proc. IEEE ICC 2014,* June, 2014.

[9] S. Sun, et. al., "Millimeter Wave Multi-beam Antenna Combining for 5G Cellular Link Improvement in New York City," *in Proc. IEEE ICC 2014*, June 2014.

[10] M. Kyrö, et. al., "Experimental propagation channel characterization of mm-wave radio links in urban scenarios," *IEEE Antennas and Wireless Propagation Letters,* Vol. 11, 2012.

[11] S. G. Larew, et. al., "Air interface design and ray tracing study for 5G millimeter Wave communications," *in Proc. IEEE Globecom2013-B4G Workshop*, December 2013.

[12] M. R. Akdeniz, et. al., "Millimeter wave channel modeling and cellular capacity evaluation," *IEEE Journal on Sel. Areas in Comm*., Special Issue on 5G, July, 2014.

[13] Y. Azar, et. al., "28 Ghz propagation measurements for outdoor cellular communications using steerable beam antennas in new york city," *in Proc. IEEE ICC 2013*, June 2013.

[14] H. C. Nguyen, et. al., "Evaluation of empirical ray-tracing model for urban outdoor scenario at 73 GHz", *in Proc. IEEE VTC Fall 2014*.

[15] T. A. Thomas, et. al., "3D extension of the 3GPP/ITU channel model," *in Proc. IEEE VTC-Spring 2013*, June 2013.

[16] N. Czink and P. Cera, "A novel rramework for clustering parametric MIMO channel data including MPC powers," *in COST 273 post-Project Meeting*, Lisbon, Portugal, Nov. 2005.

[17] M. Kyrö, et. al., "Long range wideband channel measurements at 81-86 GHz frequency range," *in Proc. EuCAP 2010*, April 2012.

[18] A. Maltsev, et. al., "Impact of polarization characteristics on 60-GHz indoor radio communication systems," *IEEE Antennas and Wireless Propagation Letters*, Vol. 9, pps. 413-416, 2010.

[19] T. S. Rappaport, D. A. Hawbaker, "Wide-band microwave propagation parameters using circular and linear polarized antennas for indoor wireless channels," *IEEE Trans. on Comm*., Vol. 40, No. 2, February 1992, pp. 240-245.

TABLE I. MMWAVE URBAN MICRO (UMI) CHANNEL MODEL PARAMETERS
(*d* in equations is the 3D distance in m)

		mmWave-UMi
Delay spread (σ_τ) $\log_{10}$(seconds)	μ_{DS}	-6.8
	ε_{DS}	0.3
Delay distribution		Exponential
Delay scaling parameter, r_τ		3
AoD spread (σ_{ASD}) $\log_{10}$(degrees)	μ_{ASD}	1.1
	ε_{ASD}	0.42
AoA spread (σ_{ASA}) $\log_{10}$(degrees)	μ_{ASA}	1.3
	ε_{ASA}	0.36
ZoD spread (σ_{ZSD}) $\log_{10}$(degrees)	μ_{ZSD}	max(-0.002*d*+1.05,0.4)
	ε_{ZSD}	0.32
ZoA spread (σ_{ZSA}) $\log_{10}$(degrees)	μ_{ZSA}	max(-0.0025*d*+1.1,0.3)
	ε_{ZSA}	0.26
ZoD bias ($\mu_{bias,ZoD}$) $\log_{10}$(-degrees)	μ_{ZBD}	max(-0.0022*d*+1.36,0.6)
	ε_{ZBD}	0.3
ZoA bias ($\mu_{bias,ZoA}$) $\log_{10}$(-degrees)	μ_{ZBA}	Max(-0.0017*d*+1.09,0.4)
	ε_{ZBA}	0.3
AoD and AoA distribution		Wrapped Gaussian
ZoD and ZoA distribution		Laplacian
LOS shadow fading	σ_{SF}	4.9 dB
NLOS shadow fading	σ_{SF}	7.6 dB
LOS Ricean K factor (dB)	μ_K	12
	ε_K	3
XPR (dB)	μ_{XPR}	15
	σ_{XPR}	2
Number of clusters		5
Number of rays per cluster		10
Cluster ASD (degrees)		6
Cluster ASA (degrees)		5.3
Cluster ZSD (degrees)		10^max(-0.0023*d*+0.81,0)
Cluster ZSA (degrees)		10^max(-0.002*d*+0.83,0)
Per-cluster shadow fading (dB)		5

TABLE II. MMWAVE CHANNEL MODEL CROSS CORRELATIONS

ASD vs. DS	0.49
ASA vs. DS	0
ASD vs. ASA	0
ESD vs. DS	0.29
ESA vs. DS	0
ESD vs. ASD	0.62
ESA vs. ASD	0
ESD vs. ASA	0
ESA vs. ASA	0.55
ESD vs. ESA	0.33
ASA vs. ZBA	0.45
ASD vs. ZBA	-0.16
DS vs. ZBA	-0.26
ESA vs. ZBA	0.69
ESD vs. ZBA	0.17
ASA vs. ZBD	0
ASD vs. ZBD	0.47
DS vs. ZBD	0.2
ESA vs. ZBD	0.33
ESD vs. ZBD	0.76
ZBA vs. ZBD	0.39

TABLE III. ANGLE OFFSETS WITHIN A CLUSTER

Ray number, *m*	Offset angle, α_m
1,2	±0.0447
3,4	±0.2492
5,6	±0.5129
7,8	±0.8844
9,10	±1.5195